Journal of Materials Chemistry

Cite this: *J. Mater. Chem.*, 2011, **21**, 7401

www.rsc.org/materials

PAPER

Preparation of porous composite ion-exchange membranes for desalination application†

Chalida Klaysom,[a] Roland Marschall,[a] Seung-Hyeon Moon,[b] Bradley P. Ladewig,[ac] G. Q. Max Lu*[a] and Lianzhou Wang*[a]

Received 29th November 2010, Accepted 15th March 2011
DOI: 10.1039/c0jm04142d

Via a two-step phase inversion technique, composite membranes with controllable porosity and a significant improvement of electrochemical properties were successfully prepared. The presence of surface functionalized mesoporous silica (SS) as inorganic fillers in the sulfonated polyethersulfone (sPES) polymer matrix was proved to have a great impact on the resultant membrane structure, which subsequently led to significantly enhanced ionic conductivity of the membranes. The correlation among inorganic fillers, composite structures, electrochemical properties and desalination performance by electrodialysis (ED) was discussed in detail. The optimal membrane was the composite with 0.2 wt% SS loading, which possessed a good ionic conductivity of 5.554 mS cm^{-1}, a high selectivity with 0.95 transport number while maintaining good mechanical strength and thermal stability. Moreover, the performance of this membrane in ED was comparable to a commercial membrane (FKE), exhibiting a current efficiency of 0.84 and 3.82 kW h kg^{-1} of salt removed.

Introduction

Ion-exchange membranes have attracted great attention from both academic and industrial fields, due to their versatile potential applications including water purification and food processing.[1–10] Many attempts have been made by a number of research groups to develop robust membranes with desirable properties for different applications. These include (1) a search for new polymers with highly modified chemical structures enhancing membrane conductivity and electrochemical properties, (2) surface and structure modification of existing commercial membranes, and (3) improvement of considerably cheaper polymer in the market by blending other polymers or incorporating some additives into the parent matrix.[11–13] Though the concept of combining two distinct materials forming a new composite that keeps desirable properties of both components has been well established, it has not been applied much in the development of ion-exchange membranes especially in desalination applications. In this work we aim to design a new type of hybrid ion-exchange membranes by introducing inorganic fillers to the sulfonated polyethersulfone (sPES) polymer matrix.

Sulfonated aromatic hydrocarbons such as sPES have been extensively used as an alternative electrodriving membrane due to their low cost, excellent mechanical, thermal and chemical stabilities. Moreover, this type of polymers is also easy to process and has been widely used as the polymer matrix alternative in replacing Nafion for composite membranes in fuel cell application.[10,14–16] A variety of inorganic fillers such as sulfonated polyhedral oligomeric silsesquioxane (sPOSS), phosphotungstic acid, boron phosphate, clay, and silica were introduced into the sPES to prepare a composite membrane by either sol–gel or blending method.[17–21] A few successful examples of composite proton-exchange membranes with improved ion-exchange capacity and conductivity suitable for fuel cell application have been reported.[17–27] For instance, Choi *et al.* recently reported the preparation of sulfonated polysulfone/sPOSS fiber composite membranes with superior ion-exchange capacity and high proton conductivity even at very low relative humidity.[17] Note that this type of membranes required several steps to prepare, which may be disadvantageous for scale-up preparation. Despite the success in composite proton exchange membrane preparation, the development of composite membranes for desalination application has been very rare. In our previous work, composite membranes containing a small amount of surface functionalized mesoporous silica (SS) in the sPES polymer matrix were prepared by a simple procedure. The resultant composite membranes exhibited enhanced electrochemical properties while still retaining excellent mechanical strength and thermal

[a]*ARC Centre of Excellence for Functional Nanomaterials, School of Chemical Engineering and Australian Institute of Bioengineering and Nanotechnology, The University of Queensland, Qld, 4072, Australia. E-mail: l.wang@uq.edu.au; Fax: +61 7 3365 4199; Tel: +61 7 3365 4218*
[b]*Gwangju Institute of Science and Technology, School of Environmental Science and Engineering, Gwangju, 500-712, Republic of Korea*
[c]*Monash University, Department of Chemical Engineering, Vic, 3800, Australia*

† Electronic supplementary information (ESI) available: Supplementary information. See DOI: 10.1039/c0jm04142d

stability.[28] However, due to the dense structure of the obtained membranes prepared by the widely used solvent evaporation method, their ionic conductivity was still very low, being incomparable with commercial membranes on the market.

In the present work, we report an innovative structural modification pathway, namely the two-step phase inversion technique, to tailor the membrane porosity of the sPES–SS composite membranes, which in turn led to significantly improved ionic conductivity for the membranes. The relationship among porosity/structure, physicochemical and electrochemical properties of the resultant membranes was investigated in detail. Encouragingly, the performance of this new type of membrane in ED desalination was comparable to that of a commercial FKE membrane.

Experimental

Material synthesis

The synthesis procedure and material characterization of sPES and SO_3H-functionalized mesoporous SiO_2 (SS) were described in more detail elsewhere.[13,28] The ion-exchange capacity of SS was measured by back titration. The structure and morphology of the SS were studied by transmission electron microscopy (TEM, JEOL 1010) and X-ray diffraction (XRD, Rigaku Miniflex) under copper radiation (CuKα, 30 kV and 15 mA).

Membrane preparation

Composite membranes were prepared by a two-step phase inversion procedure. In the first step, a polymer solution consisting of 25 wt% sPES in dimethylformamide (DMF, Sigma) was prepared, and then various amounts of SS (0–2 wt%) were added into the polymer solutions at 60 °C for 4 h under stirring. Sonication was applied to the mixture solution before it was cast on glass substrates using a doctor blade with a casting thickness of *ca.* 0.40 mm. In the second step, the cast film was dried in a vacuum oven at 60 °C for 10 min and then precipitated in a 60–70 °C DI water bath. The formed membrane sheet was peeled off from the glass substrate and kept in DI water. A series of membranes were named by considering the wt% of SS added into the polymer matrix. For instance, 0.2SS represents the composite membrane of sPES containing 0.2 wt% of SS. The prepared membranes were then treated in hot water for 2 h and then in 1 mol dm^{-3} HCl for 24 h. Subsequently, the membranes were rinsed with DI water and kept in 1 mol dm^{-3} NaCl solution. All membranes were equilibrated in working solution for at least 6 h before use.

Membrane characterization

Membrane morphology. Scanning electron microscopy (SEM, JEOL 6300) was used to observe the morphology and structure of the prepared membranes. To obtain a sharp cross-sectional surface the samples were fractured in liquid nitrogen, and then the captured water was dried out overnight in a freeze dryer to preserve their structure.

Ion-exchange capacity (IEC) and water uptake of ion-exchange membranes. Ion-exchange capacities were measured by a back titration technique. Firstly, the cation-exchange membrane was soaked in 1 mol dm^{-3} HCl for at least 6 h. After that, the membrane was washed with DI water to remove the excess HCl and then was immersed into 1 mol dm^{-3} NaCl solution for another 6 h. The number of displaced protons from the membrane was determined by titration with 0.01 mol dm^{-3} standard NaOH solution using phenolphthalein as an indicator. Then the membrane was soaked in DI water for 24 h or more. Afterward, the membrane was taken out and the excess water on the surface was removed with tissue paper. The wet weight of membrane was measured. Then the membrane was dried at 50 °C in an oven for 10 h or until there were no weight changes in the membranes. The dry weight of the membrane was recorded. The IEC and water uptake of membranes were then calculated using eqn (1) and (2):

$$\mathrm{IEC} = \frac{ab}{W_{\mathrm{dry}}} \tag{1}$$

$$\text{Water uptake} = \frac{W_{\mathrm{wet}} - W_{\mathrm{dry}}}{W_{\mathrm{dry}}} \tag{2}$$

where a is the concentration of NaOH solution (mol dm^{-3}), b is the volume of NaOH solution used (dm^3), W_{dry} is the dry weight of the membrane and W_{wet} is the wet weight of the membrane.

Electrochemical properties of ion-exchange membranes

Membrane resistance. The resistance of membranes was measured by impedance spectroscopy (IS) using a Solarton 225B. The working ion-exchange membrane was equilibrated in 0.5 mol dm^{-3} NaCl before being placed in a two-compartment cell between platinum electrodes with an effective area of 1 cm^2. The test was carried out in a frequency range of 1–10^6 Hz with an oscillating voltage of 100 mV.[29] The resistance corresponding to the phase angle closest to zero in the Bode diagram was recorded. Then, the membrane resistance (R_{mem}) was calculated by subtraction of the electrolyte resistance (R_{sol}) from the membrane resistance equilibrated in the electrolyte solution (R_{cell}), according to the equation $R_{\mathrm{mem}} = R_{\mathrm{cell}} - R_{\mathrm{sol}}$. The conductivity of membranes (σ, S cm^{-1}) was then calculated by eqn (3):\displaystyle

$$\sigma = \frac{L}{R_{\mathrm{mem}} A} \tag{3}$$

where R_{mem} was the resistance of membranes, L is the thickness of membranes (cm), and A is the effective area of the membranes (cm^2).

Membrane potential and transport number. The membrane potential was measured with dilute solutions in order to render negligible the activity coefficient of the electrolyte.[30] The investigated membrane was placed in a two-compartment cell, separating two NaCl concentration solutions of 0.01 mol dm^{-3} and 0.05 mol dm^{-3}, respectively. The potential difference (E_{m}) across the membrane was measured at room temperature using a multimeter which was connected to two Ag/AgCl reference electrodes. The transport number, $\bar{t}_i$, was calculated by the following equation:[4]

$$E_m = \frac{RT}{F}(2\bar{t}_i - 1)\ln\left(\frac{C_1}{C_2}\right)_i \quad (4)$$

where R is the gas constant, F is the Faraday constant, T is the absolute temperature, C_1 and C_2 are the concentrations of electrolyte solutions in the testing cell, respectively.

*Current–voltage (*i–v*) characteristic and chronopotentiometry.* The *i–v* curve and chronopotentiogram of the membranes in 0.025 mol dm^{-3} NaCl were measured at room temperature using the same two-compartment cell. The cell was connected to a Solartron Multistat 1480 by two Pt electrodes. For *i–v* curves, a stepwise potential difference was applied across the membrane and the corresponding current was measured. The chronopotentiogram was carried out at a constant applied current density of 3 mA cm^{-2} and the corresponding potential was recorded every 1 s for a period of 300 s automatically.

Thermal and mechanical stabilities of membranes

Thermal stabilities. Thermogravimetric analysis (TGA) (Mettler Teledo) was used to study the thermal stability of the membranes in the temperature range of 25–800 °C with a heating rate of 10 °C min^{-1} under a nitrogen flow of 20 cm^3 min^{-1}.

Mechanical properties. The mechanical properties of wet membranes were measured by the tensile test at room temperature using an Instron 5800 at a speed of 2 mm min^{-1}. The tested samples were equilibrated in DI water for 24 h and then cut into a rectangular shape with dimensions of 50 mm × 5 mm. The gauge length of each specimen was 14 mm. At least five specimens from each sample were tested.

Desalination by electrodialysis

The performance of the prepared membranes was tested in a custom designed ED cell. The cell consists of 5-compartment chamber made of Perspex sheet. Each chamber provides 4 cm^2 active area for membranes with an o-ring to prevent leakage during the testing. The scheme of the ED setup and the membrane configuration in the cell are illustrated in Fig. 1.

The ED of NaCl solution was carried out with potentiostatic modes. The feed solution (150 cm^3 of 0.2 mol dm^{-3} NaCl) was circulated at 30 cm^3 min^{-1} through the dilute and concentrated compartments. The concentrated compartments were adjacent to the electrode rinse compartments in which 150 cm^{-3} of 3 wt% Na_2SO_4 was circulated at 30 cm^3 min^{-1}. The commercial cation-exchange membranes FKE were placed at the positions C_1 and C_3 in Fig. 1(a) next to the electrode to separate the electrode solution from the product solution. The composite membrane as a cation-exchange membrane was placed in position C_2 and commercial anion-exchange membrane was placed in position A to complete the cell. The performances of the prepared membranes were compared with the commercial membrane in terms of flux, current efficiency and energy consumption calculated by the following equations.

$$\text{Flux} = \frac{\Delta N}{At} \quad (5)$$

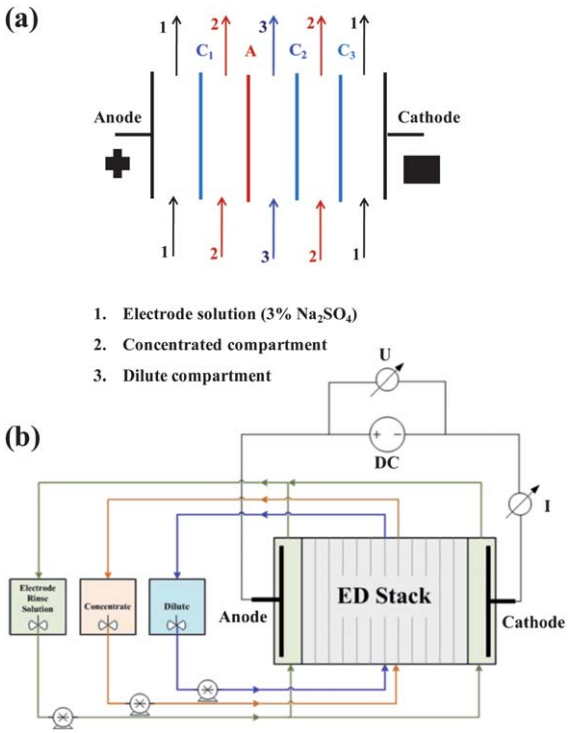

Fig. 1 ED cell configuration (a) and schematic diagram of the test in ED system (b).

$$\eta = \frac{Fz\Delta N}{n_c \int I\mathrm{d}t} \quad (6)$$

$$P = \frac{FzU}{3600\eta M_{\text{Nacl}}} \quad (7)$$

where η = current efficiency of the dilute, F = Faraday constant (96 487 As mol^{-1}), $\Delta N = C_d^{n-1}V_d^{n-1} - C_d^{n}V_d^{n}$ (mole), C_d = concentration of dilute (mol dm^{-3}), V_d = volume of the dilute (dm^{-3}), P = power consumption of NaCl (kW h kg^{-1}), n_c = number of cell pair, I = current (A), U = applied voltage (V), M_{NaCl} = molecular weight of NaCl (58.45 g mol^{-1}), A = active surface area (cm^2), and t = time (s).

The ion concentration from each compartment was determined by a conductometer and the pH of solution from each chamber was measured to indicate the water electrolysis that may occur during the process. The volume change in each reservoir was recorded at the start and end of the experiment.

Results and discussion

Structure influence of the inorganic fillers on composite properties

Following the same procedure in our previous work,[22] the SS with a particle size of 100–150 nm was firstly synthesized. The highly ordered mesoporous materials were evidenced by TEM images (Fig. 2(b and c)). Moreover, the small angle XRD of as-synthesized sulfonated SiO_2 showed well resolved reflections of 2D-hexagonal mesostructure with indexes of (100), (110), (200), and (210), confirming the highly ordered pore structure of the particles. The ion-exchange capacity of the SS particle was

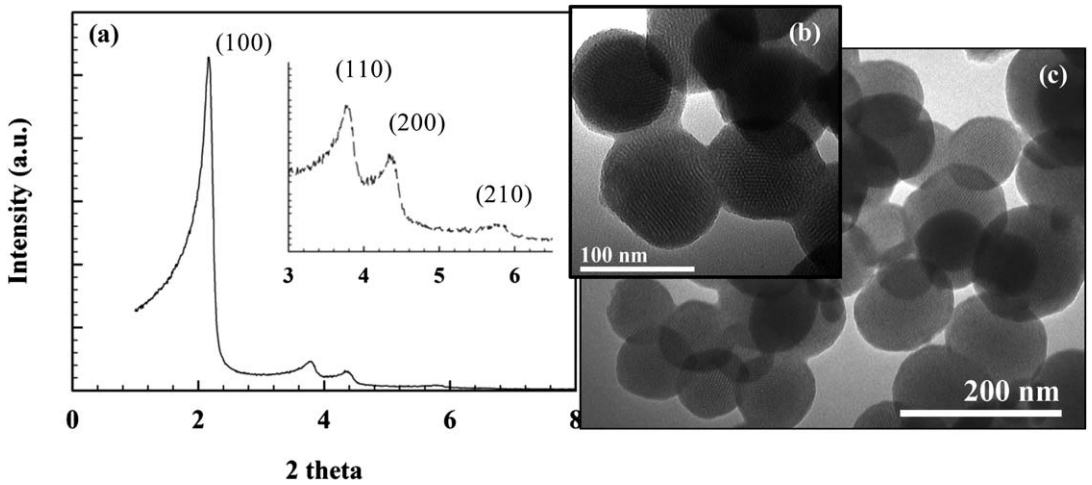

Fig. 2 Small angle XRD patterns (a) and TEM (b and c) images of sulfonated mesoporous silica (SS) at different magnifications.

estimated to be 1.8 mequiv g^{-1} by back titration, which is consistent with those reported in previous works.[13,28]

The SS particles were first mixed with polymer solution of sPES and DMF, followed by the two-step phase inversion process to form membrane sheets.[31] FTIR spectrum was used to investigate the chemical structure of each component and possible intermolecular interaction. As shown in Fig. S1†, IR vibration bands at around 1140 and 1205 cm^{-1}, characteristics of SO_3H groups attached to the silica, and at 1030 cm^{-1} for sulfonate groups of sPES were observed. These indicate the presence of ion-exchangeable groups in both sPES and SS components. However, the FTIR bands of the SS could not be clearly identified in the composite, possibly due to the very small proportion of SS in the composite or band position overlapping of the components.[32]

The morphology of the obtained composites was shown to be highly porous (Fig. 3). Compared to the pristine membrane, the presence of additives increased the porosity of the membranes. Not only the porosity of the membranes increased with SS loading, but also the pore size of the membrane. At higher loading the SS particle tends to form clusters, thus resulting in a bigger pore size. Though the SS cluster formation became more pronounced at high percentage of SS loading, these primary clusters were still well distributed throughout the entire structure of the polymer matrix.

The key properties of ion-exchange membranes including water uptake, IEC, conductivity and transport number were summarized in Table 1. As mentioned earlier, incorporating high surface functionalized silica was expected to improve the IEC and water uptake and thus enhances the conductivity and transport properties of the membranes. The water uptake of the membrane was significantly improved due to three main effects of the additives; the additional hydrophilic functional groups carried by the high surface area SS, the inherit property of silica to keep both physical and chemically bound moisture, and pore formation of the membrane contributed by SS, creating free space to absorb more water.[33] Since water channel promotes the migration of the ionic species, the conductivity of the membrane increased, following the same trend of the water uptake. Likewise, the IEC of the membrane increased with increasing the loading amount of SS and peaked at low percentage (around 0.2 wt%) of SS. The decrease of IEC when more SS was added may be due to the interaction among functional groups of the inorganic filler clusters, because agglomeration of fillers can cause the loss of the accessibility of the functional groups in SS and thus the decrease of IEC, resulting in lower water content. In

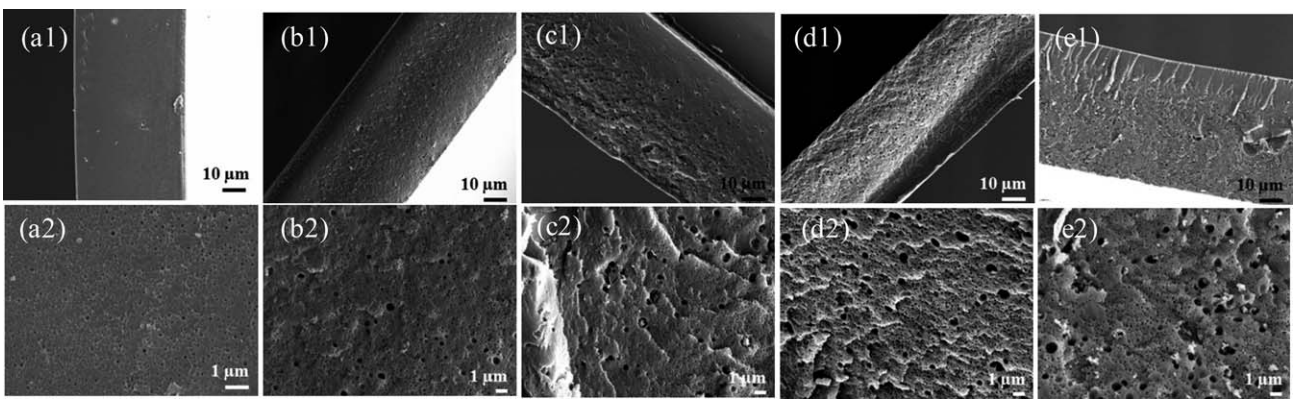

Fig. 3 SEM images of (a1 and 2) sPES membranes, (b1 and 2) composites with 0.2 wt% SS, (c1 and 2) 0.5 wt% SS, (d1 and 2) 1 wt% SS, and (e1 and 2) 2 wt% SS.

Table 1 Physicochemical and electrochemical properties of the prepared membranes compared with commercial membranes

Name	Water uptake (%)	IEC/mequiv g^{-1}	σ/mS cm^{-1}	Transport number	Free volume fraction
0SS	38.67	0.75	0.336	0.90	0.433
0.2SS	92.00	0.83	5.554	0.95	0.74
0.5SS	85.00	0.78	1.460	0.95	0.70
1.0SS	79.00	0.73	1.330	0.96	0.69
2.0SS	55.00	0.69	0.960	0.91	0.67
FKE[a]	48.10	1.20	3.834	0.95	NA

[a] A commercial cation exchange membrane from FumaTech, Germany. The FKE is made of sulfonated poly(ether ether ketone). The wet thickness of the commercial membrane was 50 ± 10 μm which is similar to those prepared membranes.

addition, more inorganic agglomerate (>1wt% SS) in the composite means reduced proportion of sPES in the membrane. Thus the ion-exchangeable functional groups contributed from sPES could also be reduced. For these reasons, the increased inorganic fillers and pore cavity did not lead to better membrane performance. The pore volume or free volume fraction in the composite membranes again suggests the optimal condition of 0.2 wt% SS, calculated by the following equation:

$$\text{Free volume fraction} = \frac{\rho_{\text{wet}} - \rho_{\text{dry}}}{\rho_{\text{w}}} \quad (8)$$

where ρ_{wet}, ρ_{dry} and ρ_{w} are the density of wet membrane, dry membrane and water at room temperature, respectively.

The results of morphology and properties as described earlier revealed that incorporating inorganic fillers had a significant impact on the membrane structure which was also directly related to the properties of the membranes. The influence of these inorganic fillers was schematically described in Fig. 4. In the phase inversion process for membrane formation, the final structure of the membrane is determined largely by the property of the casting polymer solution and its viscosity.[34–37] The less viscous the polymer solution is, the faster the solvent/nonsolvent exchange rate is, resulting in a more porous membrane structure. The pore formation of the composite in the presence of SS may be attributed to the incompatibility between the inorganic fillers and the organic polymers, creating a polymer-poor phase. As a result, the high exchange rate of solvent/nonsolvent around the inorganic fillers creates pore cavity capturing the SS particles. When more SS was added in the polymer matrix, the particles tend to form bigger clusters and thus bigger pores were produced. It can be seen from the SEM image, at more than 1 wt % SS loading, the obvious large cavities with pore interconnection were obtained. When the inorganic fillers formed large clusters, their surface functional groups were reduced and also started to interfere with the charged functional groups of the polymer matrix. As a consequence, the physicochemical and electrochemical properties of the composite declined after reaching a maximum value.

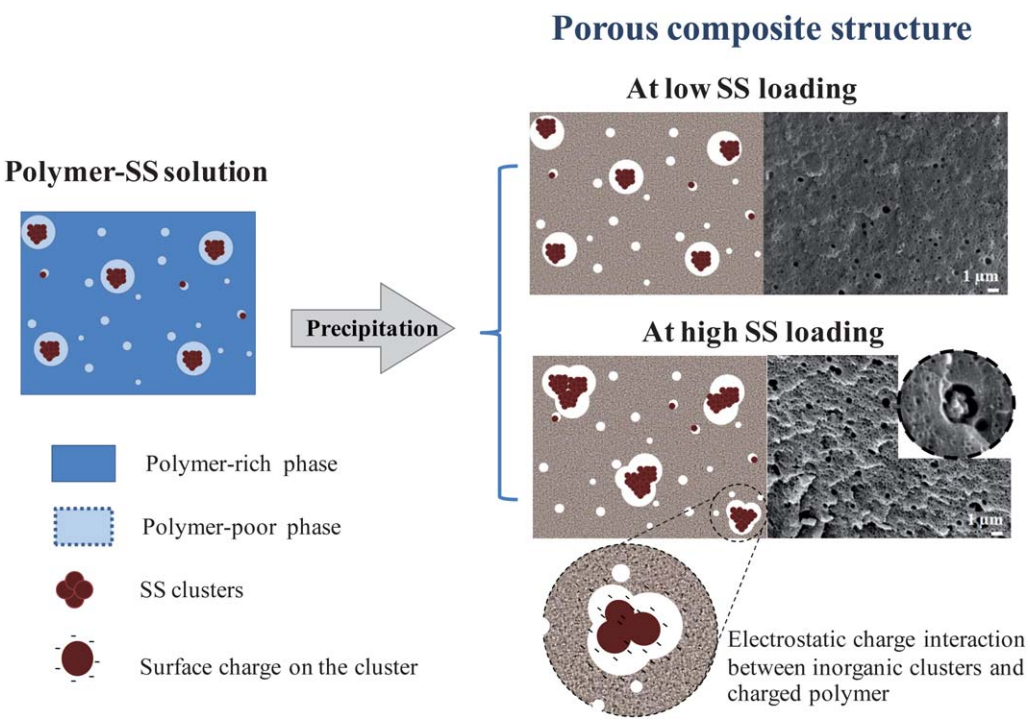

Fig. 4 Schematic diagram of pore formation with the presence of inorganic fillers and the charge interfering between inorganic clusters and polymer functional groups.

The thermal and mechanical properties of these membranes were investigated by TGA and tensile test, respectively (Fig. 5). Three-step weight loss was observed for the membranes. The first weight loss at the temperature below 100 °C is associated with the release of the absorbed moisture. Then, the slight loss at around 280 °C can be assigned to the decomposition of sulfonate groups,[38] and finally dramatic loss occurring at around 500 °C is due to the degradation of polymer chains. From the TGA curve, it is observed that the membranes exhibited a better thermal stability in the presence of inorganic fillers. This may be attributed to the interaction among the functional groups.

The mechanical testing was carried out under wet conditions and the results are presented in terms of Young's modulus, tensile stress, and strain as shown in Fig. 5(b and c). Incorporating inorganic fillers enhanced the energy distribution throughout the membranes, thus the membranes can withstand more pressure. However, in the presence of additives the membranes became more elastic and more elongated under the tensile force. As a consequence, the Young's modulus of the membranes decreased. At high degrees of loading, membranes became more brittle, resulting in the increment of the Young's modulus.

For comparison, the thermal and mechanical properties of the commercial FKE membrane, which is made of sulfonated poly (ether ether ketone), were acquired from the supplier. It was informed that the FKE possesses high thermal stability above 270 °C with a Young's modulus of 1124 MPa, a tensile stress of 36.39 MPa and a tensile strain up to 195.26% at 95% RH. Compared to the FKE membrane, our prepared membranes showed comparable thermal stability but lower mechanical stability. However, one should keep in mind that the testing conditions from the company and our experiment were different. The mechanical properties of the commercial membrane were tested under 95% RH, while our membrane was tested under the fully hydrated condition. Nevertheless, it was clear to conclude from the results of this section that our composite membranes exhibited excellent thermal stability up to 280 °C and decent mechanical strength up to 600 MPa, which are sufficient for application in desalination.

Electrochemical behavior of the composite membranes

It is of crucial importance to understand the electrochemical behavior of the membranes and to predict their performance and behavior in a real application. The electrochemical behavior of as-synthesized membranes was studied utilizing well known chronopotentiometry and current–potential (i–v) techniques.

Chronopotentiometry is a powerful tool for studying transport phenomena and concentration polarization near membrane interfaces. In this work, it was used for investigating the homogeneity of membrane surface as the ion-exchange membranes are generally considered inhomogeneous in the micro-scale consisting of conducting and non-conducting regions. By applying a constant current density to the system and measuring the corresponding potential as a function of time, the typical chronopotentiograms with three-stage potential differences were obtained and shown in Fig. 6(a). After the constant current density is applied to the system, the concentration polarization arises, resulting in the concentration gradient and slow increase of potential at the first stage. When the concentration near the membrane interface of the depleting solution decreases to nearly zero, the potential rapidly increases before reaching the steady state at the end. The time at which the potential transition occurs is called the transition time (τ). The transition time can also be expressed by the well known Sand's equation:

$$\tau = \frac{(C_0 z_i F)^2 \pi D}{4i^2(\bar{t}_i - t_i)^2} \quad (9)$$

where i is the current density, C_0 is the concentration of electrolyte, and z_i is the valence of the i^{th} ion. It is worth noting that the eqn (9) was proposed under the assumption of entire conducting surface of the membranes. The τ deprived from Fig. 6(b)

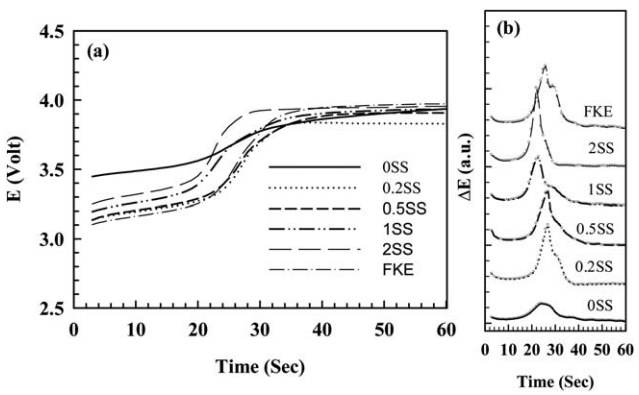

Fig. 6 Chronopotentiograms (a) and their derivative potential *vs.* time curve (b) of the synthesized membranes compared with commercial membranes tested at room temperature in 0.025 mol dm^{-3} NaCl.

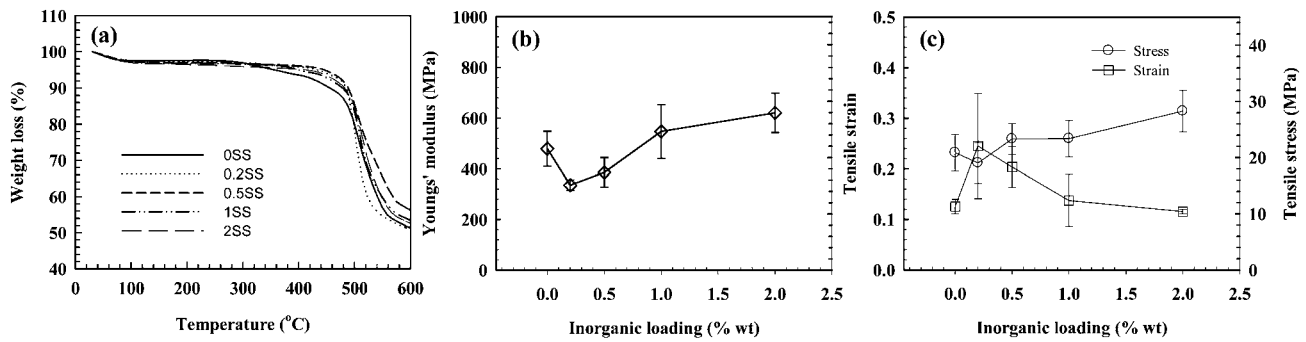

Fig. 5 Thermal (a) and mechanical properties (b: Young's modules, c: strain and stress) of the prepared membranes.

of the derivative dE/dt at the maximum value where the rapid potential increase occurred is listed in Table 2 and compared with the ideal value estimated from eqn (9). It clearly showed the deviation between those values obtained experimentally and theoretically. This can be explained by the effects of surface inhomogeniety of the membranes. Considered ion-exchange membranes as microheterogeneous membranes with reduced conducting surface, the local current density at the conducting regions is higher than the overall current density applied to the system. As a result, the time required to deplete the ionic species became shorter. The current density in the conducting region (i^*) was expressed as a function of overall current density or so-called superficial current density (i) and the fraction of the conducting region (ε) as shown below;

$$i^* = i/\varepsilon \tag{10}$$

And thus the ε can be estimated by the derived Sand's equation given as:

$$\varepsilon = \frac{2i\tau^{1/2}(\bar{t}_i - t_i)}{C_0 z_i F(\pi D)^{1/2}} \tag{11}$$

The fraction of conducting surface, ε, including all characteristic values from chronopotentiograms is summarized in Table 2. The starting potential (E_0) and the potential at the steady state (E_{max}) varied in each membrane. These characteristic values are believed to be dependent on the resistance of membranes and the testing systems. The fraction of conducting region increased with the amount of SS added and peaked at 0.2 wt% loading which is in a good agreement with the result in the previous section. The results clearly showed that the shape of chronopotentiogram and their characteristic values are highly influenced by the surface heterogeneity of the membranes. While the membrane with more surface heterogeneity (0SS) exhibits more diffused curve with more interval time (Δt) where the derivative dE/dt is not zero as can be seen in Fig. 6(b), the more surface homogeneous membranes with the presence of SS shows more defined transition time with smaller interval time.

The i–v characteristic was also used to investigate the concentration polarization of membrane interface and the limiting operating point so-called the limiting current density (LCD). By recording the corresponding current density with the stepwise potential difference, typical i–v curves of the prepared membranes were obtained as shown in Fig. 7. The linear relationship of current and potential in the beginning stage followed the Ohm's law. Subsequently, a plateau was reached when the concentration of the dilute solution near the membrane interface dropped nearly to zero due to the concentration gradient that arose from concentration polarization. The LCD can then be estimated from intersection of the tangents from these two regions. The corresponding current above the plateau region can be referred to a "so-called" over-limiting region which was believed to be influenced dominantly by the convection effects. The derivative dE/di is deprived from the original i–v curve and plotted as a function of i and E as shown in Fig. 7(b and c), respectively, in order to avoid the ambiguous estimation of the LCD from the ill-defined characteristic curve and to better visualize the plateau length. According to the concentration polarization theory, the LCD was expressed in terms of diffusion boundary layer thickness (δ), diffusion coefficient (D), and transport number as shown in eqn (12):

$$i_{lim} = \frac{|z|CFD}{\delta(\bar{t}_i - t_i)} \tag{12}$$

It is clear from the eqn (12) that under the same testing conditions, the LCD depends on the transport number of membrane. Note that the δ was considered constant in this work as this value is a function of hydrodynamic property such as feed flow or stirring rate which was also controlled in the experiment. The lower the transport number the membrane has, the higher the LCD of the membrane was expected.

However, the result showed that our composite membranes with higher transport number possessed the higher LCD. This may be attributed from the reduced conducting area of the microheterogeneous membranes explained earlier. The superficial LCD (i) deprived from Fig. 7(b) and the local LCD (i^*) of the conducting region estimated from eqn (10) were compared in Table 3. The results showed that the local LCD (i^*) is proportional to the reciprocal of the transport number of the membranes, theoretically expressed in eqn (12). It is also interesting to take a note of the plateau length of the prepared membranes that decreased with the increase of % loading and the fraction of the conducting region. The more heterogeneous the membrane surface is, the longer the plateau length is. This is consistent with reports in the literature.[4,30,39–42] However, the plateau length of composites with 2 wt% SS was much smaller than the parent membrane even though they possessed close ε values and similar properties. This may be explained by the effect of geometrical heterogeneity reported by early studies,[39,40] revealing that not only the fraction value (ε) but also the arrangement and distribution between conducting and non-conducting regions needed to be taken into account for explaining the plateau shortening or prolonging behavior. If the space distance between the two compartments is in the same magnitude with the boundary-layer thickness, the shortening plateau length of heterogeneous membranes would also be observed.

It is clear that the presence of SS fillers improved the conducting fraction of the membrane surface and consequently improved the LCD and electrochemical behavior.

Table 2 Characteristic values from chronopotentiograms

Sample	$\bar{t}_i$	τ^a/s	τ^b/s	ε	E_0/V	E_{max}/V	Δt/s
0SS	0.90	32.2	24 0	0.864	3.45	3.94	26
0.2SS	0.95	26.6	26.5	0.997	3.14	3.83	20
0.5SS	0.95	26.6	26.5	0.997	3.14	3.90	24
1SS	0.96	25.7	23.0	0.946	3.20	3.93	24
2SS	0.91	30.9	23.0	0.862	3.25	3.95	19
FKE	0.95	26.6	26.0	0.988	3.10	3.94	24

[a] Estimated from eqn (9). [b] Deprived experimentally from chronopotentiogram.

Desalination of NaCl by ED

The performance of composite membranes with 0.2 and 0.5 wt% SS in a custom-designed ED cell was evaluated and compared with the unmodified and commercial membranes. The ED test

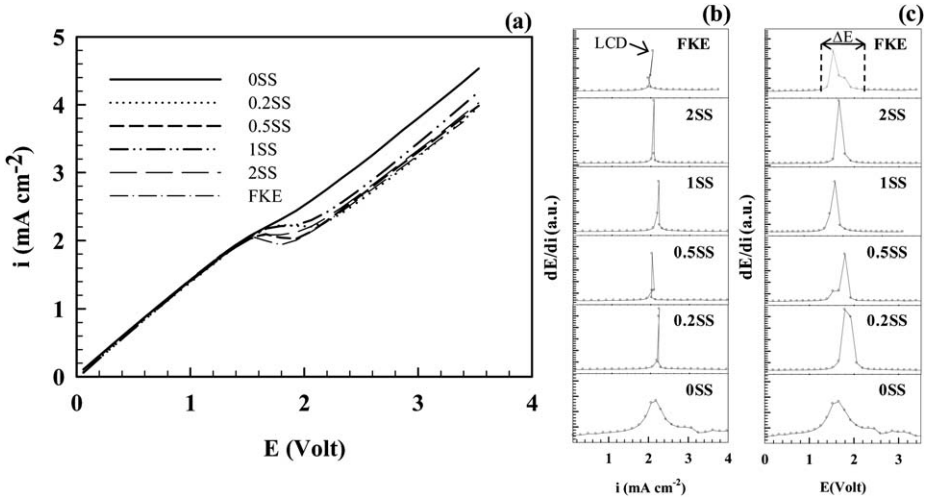

Fig. 7 *i–v* curve (a), and derivative d*E*/d*i* as a function of *i* (b) and derivative d*E*/d*i* as a function of *E* (c) of the obtained membranes measured at room temperature in 0.025 mole dm^{-3}.

Table 3 Characteristic values from *i–v* curve

Sample	*i*/mA cm^{-2}	*i**/mA cm^{-2}	Δ*E*/V
0SS	2.19	2.54	1.60
0.2SS	2.21	2.21	0.94
0.5SS	2.04	2.04	0.67
1SS	2.21	2.33	0.53
2SS	2.08	2.41	0.70
FKE	2.06	2.08	1.10

Table 4 Performance of the prepared membranes compared with benchmark in ED

Operating *E*/V	Sample	Flux/mole m^{-2} h^{-1}	η	*P*/kW h kg^{-1} salt
7	0SS	4.56	0.56	5.74
	0.2SS	6.62	0.84	3.82
	0.5SS	6.73	0.79	4.01
	FKE	7.46	0.83	3.92
5	0.5SS	4.12	0.99	2.28
	FKE	4.10	0.75	3.11

was carried out with potentiostatic mode (CV) at 7 volts. The concentration of desalting solution, pH and current density were recorded over the testing period and the results were shown in Fig. 8. The average values over the testing time of flux, current efficiency and energy consumption were then calculated and listed in Table 4. The composite membranes showed significantly better performance compared to the pristine membrane, due to the remarkable enhanced conductivity and transport properties by incorporating surface functionalized silica. It is also interesting to note that under the same testing condition, the composite membranes also show comparable performance to the benchmark membranes. Unlike the commercial membrane FKE, which experienced the pH change after 60 min of operation, our membranes were quite stable and the pH change was observed for 0.5 wt% SS after 240 min. To ensure that the pH change was not because of the chemical degradation of the membranes during the ED operation, the IR spectra of the membranes before and after ED testing were investigated (see ESI, Fig. S2†). It was clear that there were no apparent difference of the chemical structure observed. This implies that water dissociation was occurring with the commercial and 0.5SS membranes, an inappropriate testing condition for these two membranes. Therefore, the lower potential condition was used for FKE and 0.5SS membrane to avoid water splitting phenomena. The results are also shown in Table 4. In the later situation, the 0.5SS membrane performed notably better than the commercial one with 0.99 current efficiency and 2.28 kW h kg^{-1} of salts removed.

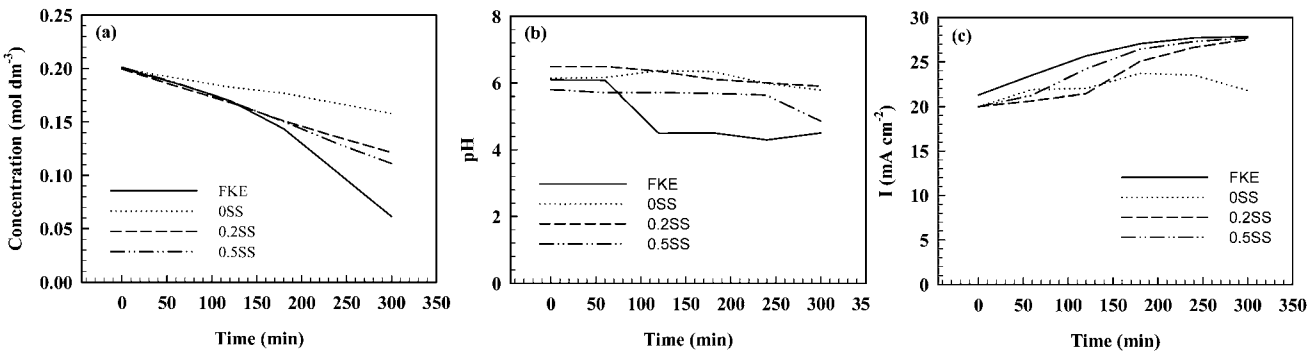

Fig. 8 Electrodialysis of NaCl solution: changes of (a) concentration, (b) pH and (c) current density *vs.* time.

As the performance of ED not only depends on membrane properties but also the testing conditions and cell design, the optimal operating condition of a given testing cell should be carefully tuned.

Conclusion

A new two-step phase inversion membrane formation technique allows a good control of the membrane structure, porosity and electrochemical properties. Such properties were found to be significantly affected by the presence of inorganic fillers. The composite membranes with 0.2–0.5 wt% of SS showed the optimum properties and performance in ED, which is comparable to the commercial benchmark membranes. Incorporating sulfonated mesoporous silica was shown to be an effective approach to enhance the performance of ion-exchange membranes. The findings from this work will lead to a better understanding of the effects of inorganic fillers on sPES membranes and provide new insights into how to develop composite ion-exchange membranes with desirable properties for desalination.

Acknowledgements

The financial support from Australian Research Council (through its ARC Centre of Excellence and Discovery programs), CSIRO Advanced Membranes for Water Treatment Cluster Project, and Thai government (through Higher Educational Strategic Scholarship for Frontier Research Network) is gratefully acknowledged. Additional thanks are due to Richard and Robyn Webb for technical support on the SEM sample preparation and TEM.

References

1 G. S. Gohil, R. K. Nagarale, V. V. Binsu and V. K. Shahi, *J. Colloid Interface Sci.*, 2006, **298**, 845–853.
2 J. Balster, O. Krupenko, I. Punt, D. F. Stamatialis and M. Wessling, *J. Membr. Sci.*, 2005, **263**, 137–145.
3 R. Scherer, A. M. Bernardes, M. M. C. Forte, J. Z. Ferreira and C. A. Ferreira, *Mater. Chem. Phys.*, 2001, **71**, 131–136.
4 M.-S. Kang, Y.-J. Choi, I.-J. Choi, T.-H. Yoon and S.-H. Moon, *J. Membr. Sci.*, 2003, **216**, 39–53.
5 A. Elattar, A. Elmidaoui, N. Pismenskaia, C. Gavach and G. Pourcelly, *J. Membr. Sci.*, 1998, **143**, 249–261.
6 Y. S. Dzyazko and V. N. belyakov, *Desalination*, 2004, **162**, 179–189.
7 S. Feng, Y. Shang, X. Xie, Y. Wang and J. Xu, *J. Membr. Sci.*, 2009, **335**, 13–20.
8 H. K. Hansen, L. M. Ottosen and A. Villumsen, *Sep. Sci. Technol.*, 1999, **34**, 2223–2233.
9 C. Iojoiu, M. Marechal, F. Chabert and J.-Y. Sanchez, *Fuel Cells*, 2005, **5**, 344–354.
10 N. N. Krishnan, H.-J. Kim, M. Prasanna, E. Cho, E.-M. Shin, S.-Y. Lee, I.-H. Oh, S.-A. Hong and T.-H. Lim, *J. Power Sources*, 2006, **158**, 1246–1250.
11 G. Chamoulaud and D. Bélanger, *J. Colloid Interface Sci.*, 2005, **281**, 179–187.
12 R. Marschall, I. Bannat, J. Caro and M. Wark, *Microporous Mesoporous Mater.*, 2007, **99**, 190–196.
13 R. Marschall, I. Bannat, A. Feldhoff, L. Wang, G. Q. M. Lu and M. Wark, *Small*, 2009, **5**, 854–859.
14 H. Dai, R. Guan, C. Li and J. Liu, *Solid State Ionics*, 2007, **178**, 339–345.
15 R. K. Nagarale, G. S. Gohil, V. K. Shahi, G. S. Trivedi and R. Rangarajan, *J. Colloid Interface Sci.*, 2004, **277**, 162–171.
16 I. S. Byun, I. C. Kim and J. W. Seo, *J. Appl. Polym. Sci.*, 2000, **76**, 787–798.
17 J. Choi, K. M. Lee, R. Wycisk, P. N. Pintauro and P. T. Matherc, *J. Electrochem. Soc.*, 2010, **157**, B154–B159.
18 V. K. Shahi, *Solid State Ionics*, 2007, **177**, 3395–3404.
19 R. K. Nagarale, W. Shin and P. K. Singh, *Polym. Chem.*, 2009, **1**, 388–408.
20 L. Li and Y. Wang, *J. Power Sources*, 2006, **162**, 541–546.
21 C. L. Buquet, K. Fatyeyeva, F. Poncin-Epaillard, P. Schaetzel, E. Dargent, D. Langevin, Q. T. Nguyen and S. Marais, *J. Membr. Sci.*, 2010, **351**, 1–10.
22 G. Alberti, M. Casciola, M. Pica and G. D. Cesare, *Ann. N. Y. Acad. Sci.*, 2003, **984**, 208–225.
23 V. V. Binsu, R. K. Nagarale and V. K. Shahi, *J. Mater. Chem.*, 2005, **15**, 4823–4831.
24 R.-Q. Fu, L. Hong and J. Y. Lee, *Fuel Cells*, 2007, **1**, 52–61.
25 C. Li, G. Sun, S. Ren, J. Liu, Q. Wang, Z. Xu, H. Sun and W. Jin, *J. Membr. Sci.*, 2006, **272**, 50–57.
26 K. Miyatake, T. Tombe, Y. Chikashige, H. Uchida and M. Watanbe, *Angew. Chem., Int. Ed.*, 2007, **46**, 6646–6649.
27 S. P. Nunes, B. Ruffmann, E. Rikowski, S. Vetter and K. Richau, *J. Membr. Sci.*, 2002, **203**, 215–225.
28 C. Klaysom, R. Marschall, B. P. Ladewig, G. Q. M. Lu and L. Wang, *J. Mater. Chem.*, 2010, **20**, 4669–4674.
29 R. K. Nagarale, G. S. Gohil and V. K. Shahi, *Adv. Colloid Interface Sci.*, 2006, **119**, 97–130.
30 J.-H. Choi, S.-H. Kim and S.-H. Moon, *J. Colloid Interface Sci.*, 2001, **241**, 120–126.
31 C. Klaysom, S.-H. Moon, B. P. Ladewig, G. Q. M. Lu and L. Wang, *J. Membr. Sci.*, 2011, **371**, 37–44.
32 M. Wilhelm, M. Jeske, R. Marschall, W. L. Cavalcanti, P. Tolle, C. Kohler, D. Koch, T. Frauenheim, G. Grathwohl, J. Caro and M. Wark, *J. Membr. Sci.*, 2008, **316**, 164–175.
33 L. Chazeau, C. Gauthier, G. Vigier and J. Y. Cavaille, in *Handbook of Organic–Inorganic Hybrid Materials and Nanocomposites*, ed. H. S. Nalwa, American Scientific Publishers, 2003, vol. 2, Nanocomposites, pp. 63–111.
34 C. Barth, M. C. Goncalves, A. T. N. Pires, J. Roeder and B. A. Wolf, *J. Membr. Sci.*, 2000, **169**, 287–299.
35 J. Barzin and B. Sadatnia, *Polymer*, 2007, **48**, 1620–1631.
36 A. Conesa, T. Gumi and C. Palet, *J. Membr. Sci.*, 2007, **287**, 29–40.
37 P. Van de Witte, P. J. Dijkstra, J. W. A. Van de Berg and J. Feijen, *J. Membr. Sci.*, 1996, **117**, 1–31.
38 A. Noshay and L. M. Robeson, *J. Appl. Polym. Sci.*, 1976, **20**, 1885–1903.
39 J. Balster, M. H. Yildirim, D. F. Stamatialis, R. Ibanez, R. G. H. Lammertink, V. Jordan and M. Wessling, *J. Phys. Chem.*, 2007, **111**, 2152–2165.
40 R. Ibanez, D. F. Stamatialis and M. Wessling, *J. Membr. Sci.*, 2004, **239**, 119–128.
41 N. Pismenskaya, P. Sistat, P. Huguet, V. Nikonenko and G. Pourcelly, *J. Membr. Sci.*, 2004, **228**, 65–76.
42 V. M. Aguilella, S. Mafe, J. A. Manzanares and J. Pellicer, *J. Membr. Sci.*, 1991, **61**, 177–190.